



**HAL**  
open science

# Strong Influence of Decoherence Corrections and Momentum Rescaling in Surface Hopping Dynamics of Transition Metal Complexes

Felix Plasser, Sebastian Mai, Maria Fumanal, Etienne Gindensperger, Chantal Daniel, Leticia González

► **To cite this version:**

Felix Plasser, Sebastian Mai, Maria Fumanal, Etienne Gindensperger, Chantal Daniel, et al.. Strong Influence of Decoherence Corrections and Momentum Rescaling in Surface Hopping Dynamics of Transition Metal Complexes. *Journal of Chemical Theory and Computation*, 2019, 15 (9), pp.5031-5045. 10.1021/acs.jctc.9b00525 . hal-03037918

**HAL Id: hal-03037918**

**<https://hal.science/hal-03037918>**

Submitted on 14 Dec 2020

**HAL** is a multi-disciplinary open access archive for the deposit and dissemination of scientific research documents, whether they are published or not. The documents may come from teaching and research institutions in France or abroad, or from public or private research centers.

L'archive ouverte pluridisciplinaire **HAL**, est destinée au dépôt et à la diffusion de documents scientifiques de niveau recherche, publiés ou non, émanant des établissements d'enseignement et de recherche français ou étrangers, des laboratoires publics ou privés.

# Strong Influence of Decoherence Corrections and Momentum Rescaling in Surface Hopping Dynamics of Transition Metal Complexes

Felix Plasser,<sup>\*,†,¶</sup> Sebastian Mai,<sup>†</sup> Maria Fumanal,<sup>‡</sup> Etienne Gindensperger,<sup>‡</sup>  
Chantal Daniel,<sup>‡</sup> and Leticia González<sup>†</sup>

<sup>†</sup>*Institute for Theoretical Chemistry, Faculty of Chemistry, University of Vienna,  
Währingerstr. 17, 1090 Vienna, Austria*

<sup>‡</sup>*Laboratoire de Chimie Quantique, Institut de Chimie Strasbourg, UMR7177  
CNRS/Université de Strasbourg 4 Rue Blaise Pascal BP296/R8, F-67008 Strasbourg,  
France*

<sup>¶</sup>*Department of Chemistry, Loughborough University, Loughborough, LE11 3TU, U.K.*

E-mail: f.plasser@lboro.ac.uk

## Abstract

The reliability of different parameters in the surface hopping method is assessed for a vibronic coupling model of a challenging transition metal complex, where a large number of electronic states of different multiplicities are met within a small energy range. In particular, the effect of two decoherence correction schemes and of various strategies for momentum rescaling and treating frustrating hops during the dynamics is investigated and compared against an accurate quantum dynamics simulation. The results show that small differences in the surface hopping protocol can strongly affect the results. We find a clear preference for momentum rescaling along the nonadiabatic coupling vector and trace this effect back to an enhanced number of frustrated hops. Furthermore, reflection of the momentum after frustrated hops is shown to work better than to ignore the completely. The study also highlights the importance of the decoherence correction but neither of the two methods employed, energy based decoherence and augmented fewest switches surface hopping, performs completely satisfactory. More generally, the study emphasises the im-

portance of the often neglected parameters in surface hopping and shows that there is still need for simple, robust, and generally applicable correction schemes.

## 1 Introduction

Many important processes in photochemistry and electrochemistry are governed by nonadiabatic transitions between electronic states,<sup>1-6</sup> at which the Born-Oppenheimer approximation breaks down, meaning that electronic and nuclear degrees of freedom can no longer be separated. The surface hopping dynamics method<sup>7</sup> has become a popular approach to describe nonadiabatic processes due to its conceptual simplicity and the intuitive interpretation of the results in a quasi-classical picture. As a result, surface hopping is widely applied in many different application areas and ~~and~~ a large body of recent work exists.<sup>3,8-15</sup> The simplicity of the classical picture is deceptive as it nevertheless needs to mimic non-trivial underlying quantum processes, such as (i) the branching of the wavepacket onto different electronic states, (ii) the loss of electronic coherence due to interactions with the nuclei or the environment, (iii)

the exchange of energy and momentum between electronic and nuclear degrees of freedom, and (iv) classically forbidden transitions.

Point (i) is treated by the surface hopping algorithm itself meaning that rather than describing the whole wavepacket branching onto different potential energy surfaces (PES), one of the surfaces is selected by using a stochastic algorithm and only this branch is further propagated; an ensemble of trajectories following the different branches is then needed to resemble a bifurcating quantum wavepacket. The fact that only one branch is propagated, automatically means that it is not possible to model the interactions between different branches and their eventual loss of coherence (ii), and this has led to the introduction of decoherence corrections on top of the surface hopping algorithm.<sup>16–20</sup> An exchange of energy and momentum (iii) should occur during surface hops and different schemes of redistributing energy and momentum have been developed. Here, a new complication (iv) comes into play if the quantum and classical descriptions lead to incompatible results and the quantum propagation requires a classically forbidden hop, also called a "frustrated hop".<sup>18,21</sup> In order to deal with the above-mentioned formal problems as well as additional numerical problems<sup>22</sup> a number of different flavours of the surface hopping method have been developed,<sup>9,12,14,23</sup> able to work under different circumstances.

While surface hopping simulations can depend strongly on the electronic structure method employed for the underlying on-the-fly calculations,<sup>24,25</sup> it is often forgotten that changes in the surface hopping algorithm can also have its consequences. The reliability of surface hopping algorithms has been tested particularly on idealized model systems, such as spin-boson models,<sup>26–28</sup> a quantum oscillator,<sup>29</sup> a two-level system in a classical bath,<sup>30</sup> or on low-dimensional scattering problems<sup>31–33</sup> and the one-dimensional LiH system.<sup>34</sup> There also exist a few studies using realistic high-dimensional PES via on-the-fly dynamics,<sup>18,35–37</sup> but in this case it is more challenging to find an accurate reference to compare with. Generally speaking, the validity

of surface-hopping could be only assessed on simple systems where accurate reference values are available. In contrast, a reference for realistic large systems is much more difficult to obtain.

In this paper, we introduce a new and generally applicable strategy to assess the quality of surface hopping on complex large systems using high-dimensional, ~~many~~ state vibronic coupling models. Since their introduction in the 80s,<sup>38</sup> vibronic coupling models have been very successful<sup>39–44</sup> in reproducing experimental work, particularly in combination with the multiconfigurational time-dependent Hartree (MCTDH) method.<sup>45–47</sup> Recently, we implemented an algorithm to perform surface hopping based on vibronic coupling models,<sup>48</sup> and showed that it can be extremely cheap computationally while still capturing the main features of a variety of photophysical processes. Here, we shall use a linear vibronic coupling (LVC) model ~~to~~ compare the results of surface hopping against an accurate ~~MCTDH~~ reference for  $[\text{Re}(\text{im})(\text{CO})_3(\text{phen})]^+$  (im = imidazole, phen = phenanthroline, see Fig. 1) ~~to~~

The choice of a transition metal complex ~~as~~ a test bed is purposely, as such systems feature a high number of excited electronic states of different multiplicities in a limited domain of energy and the description of its dynamics represent a particularly challenging case for spin-vibronic models.<sup>49</sup> Moreover, the dynamics of  $[\text{Re}(\text{im})(\text{CO})_3(\text{phen})]^+$  is particularly rich, as due to the presence of an intermediate intra-ligand triplet state  ${}^3\text{IL}$  ( $T_3$ ) that couples strongly with the initially populated second singlet metal-to-ligand charge transfer  ${}^1\text{MLCT}$  ( $S_2$ ) state, spin-orbit coupling (SOC) effects are dominant at the early time of the dynamics ( $< 50$  fs) while vibronic effects lead to populate the lowest  ${}^3\text{MLCT}$  ( $T_1$ ) state by exchange with  ~~$T_3$ .~~<sup>?</sup> Depending on the character and relative positions of the low-lying states the early time spin-vibronic mechanism will be driven essentially either by vibronic effects<sup>43,50</sup> or by SOC effects.<sup>51</sup>

Studies based on the LVC model performed on a series of rhenium (I) carbonyl  $\alpha$ -diimine complexes revealed the dominant normal modes and associated (spin) vibronic couplings that

drive the ultra-fast decay ( $< 200$  fs) within the low-lying singlet and triplet states.<sup>43,50–53</sup> Previous simulations on  $[\text{Re}(\text{im})(\text{CO})_3(\text{phen})]^+$  showed that the key normal modes are the phen and carbonyl vibrations whereas the imidazole ligand is a spectator.<sup>54</sup> Here we employ a model of 2 singlet and 4 triplet states, vibronically coupled via 15 normal modes, as well as three additional models with a reduced set of electronic states. In each case, 13 different surface hopping protocols are compared to the MCTDH reference. The 200 trajectories propagated over 500 fs are equivalent to a total of more than ten million formal electronic structure computations. Doing this would be hardly feasible with on-the-fly dynamics but it requires negligible computational effort with our new implementation of LVC<sup>48</sup> in the SHARC (surface hopping including arbitrary couplings)<sup>55,56</sup> dynamics package.<sup>57</sup>

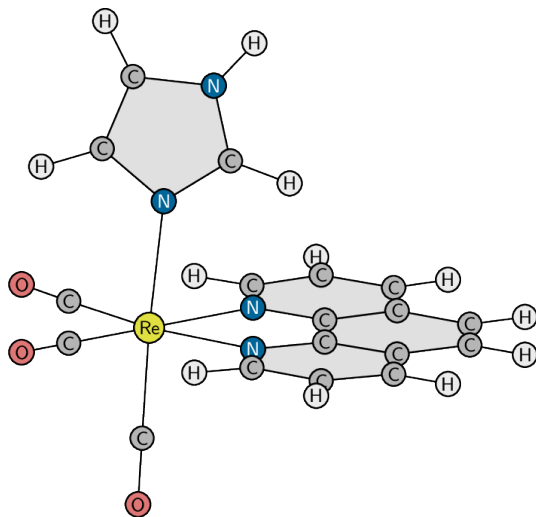


Figure 1: Chemical structure of the  $[\text{Re}(\text{im})(\text{CO})_3(\text{phen})]^+$  complex studied within this work.

## 2 Methods

Here we review essential aspects of surface hopping, such as the representations for the electronic wavefunctions, the LVC approximation, and the methodological details of the surface hopping algorithm investigated in this work, i.e. decoherence corrections, momentum rescaling and frustrated hops.

### 2.1 Wavefunction representations

An important ingredient of SHARC is the optimal use of the possible representations of the electronic wavefunctions.<sup>9</sup> To ease the discussion, we establish here the name conventions employed,<sup>9,55,56</sup> see Figure 2. Most quantum chemistry codes work with an electronic Hamiltonian that includes molecular Coulomb interactions but neither external fields nor SOC. We label this operator the molecular Coulomb Hamiltonian (MCH) and its eigenfunctions form the MCH basis (Figure 2 (b)). In this representation, states possessing distinct multiplicity are labelled as  $S_1, S_2, \dots, T_1, T_2, \dots$ . States of the same spin-multiplicity do not cross in a one-dimensional picture whereas states of different multiplicities do. The MCH states can be transformed ~~as to minimise nonadiabatic interactions~~, leading to states of almost constant character, known as diabatic<sup>38,58,59</sup> (Figure 2 (a)). These diabatic states are labelled according to their state character, e.g.  $1^1\text{MLCT}$  and  $2^1\text{MLCT}$ . The Hamiltonian including SOC is termed the "total Hamiltonian" and its eigenfunctions, generally possessing mixed spin, are the basis of what we call the "diagonal" representation<sup>55</sup> (Figure 2 (c)). These states do not cross in a one-dimensional picture.

It is important to realise that while the diabatic and MCH pictures feature ~~a single~~ PES for every triplet state, the diagonal representation considers explicitly ~~the three individual surfaces composing the triplet state~~.

The LVC model (see Section 2.2) is constructed in a diabatic basis so that it can be directly used in MCTDH.<sup>47</sup> In contrast, SHARC expects input in the MCH representation and propagates the wavefunction in the diagonal picture. It is, thus, necessary to transform the LVC states into the MCH representation before feeding this data into SHARC, as described in Ref. 48. The output from SHARC can be transformed back into any of the three pictures. In this way, it is possible to perform a one-to-one comparison between SHARC and MCTDH despite the fact that different representations are used for the wavefunction propagation.

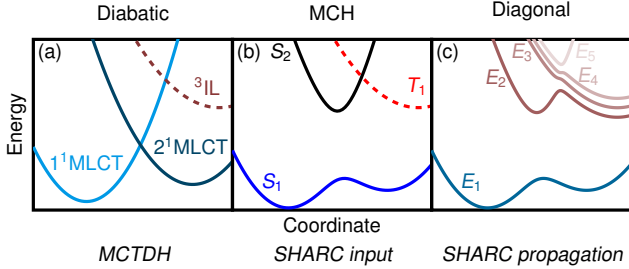


Figure 2: Wavefunction representations used in this work: (a) the diabatic representation, which is the basis for the LVC model and used for MCTDH dynamics, (b) the MCH representation, which is used by typical quantum chemistry codes and is the input for SHARC, and (c) the diagonal representation, which is used for SHARC propagations.

## 2.2 The linear vibronic coupling model

Within a vibronic coupling model, the PES are constructed in the diabatic representation, cf. Fig. 2, as

$$\mathbf{V} = V_0\mathbf{1} + \mathbf{W}, \quad (1)$$

where  $V_0$  is the ground state potential and the  $\mathbf{W}$  matrix collects the state-specific vibronic coupling terms.

The ground state potential is harmonic and given as

$$V_0 = \sum_i \frac{\hbar\omega_i}{2} Q_i^2. \quad (2)$$

Here,  $Q_i$  is a dimensionless mass-frequency scaled normal coordinate (cf. Ref. 58) defined as

$$Q_i = \sqrt{\frac{\omega_i}{\hbar}} \sum_{\alpha} K_{\alpha i} \sqrt{M_{\alpha}} r_{\alpha}, \quad (3)$$

where  $\omega_i$  is the frequency of normal mode  $i$ ,  $M_{\alpha}$  is an atomic mass, and  $K_{\alpha i}$  denotes the orthogonal conversion matrix between mass-weighted Cartesian and normal coordinates.

Within the current work, a linear vibronic coupling model (LVC) is considered, which contains the following state-specific terms in the  $\mathbf{W}$

matrix.

$$W_{nn} = \epsilon_n + \sum_i \kappa_i^{(n)} Q_i \quad (4)$$

$$, W_{mn} = \sum_i \lambda_i^{(m,n)} Q_i. \quad (5)$$

The  $\epsilon_n$  are the vertical excitation energies. The  $\kappa_i^{(n)}$  and  $\lambda_i^{(m,n)}$  are termed intrastate and interstate vibronic coupling constants.<sup>38</sup> Here these parameters were constructed from gradients and Hessian matrices, as described elsewhere,<sup>51,52</sup> while we have also shown that wavefunction overlaps can be used effectively for this purpose.<sup>53</sup> In addition, diabatic SOC constants were included as off-diagonal coupling terms, as outlined in Ref. 51. All quantities required by the SHARC dynamics program can be constructed on-the-fly by means of straightforward matrix operations, as detailed in Ref. 48.

## 2.3 Decoherence corrections

Decoherence is a fundamental concept in our understanding of how a system governed by the laws of quantum mechanics can effectively behave classically.<sup>60,61</sup> In the context of surface hopping dynamics decoherence comes into play whenever the electronic wavepacket splits into two different PES. For illustration, let us consider an electronic wavepacket propagating on two coupled PES with different nuclear gradients, see Fig. 3. Initially, the components on the upper and lower surfaces start in the same region in space. However, while the component of the wavepacket on the upper surface moves at constant speed, the part on the lower surface accelerates. As a consequence, the two parts of the wavepacket no longer occupy the same region of space, leading to loss of coherence. If the system is simulated through surface hopping dynamics, only one branch of the wavepacket, for example the one on the upper surface, is explicitly propagated for each individual trajectory. The nuclear coordinates on the second surface, indicated by empty squares in Fig. 3, are artificially fixed to match those of the first branch. As a consequence, in standard surface hopping decoherence is not treated cor-

rectly and a decoherence correction is usually included. In this work, we examine the effect of two types of decoherence corrections. One is the energy based decoherence (EDC) scheme of Grannucci et al.<sup>18</sup> –based on earlier work from Truhlar and co-workers<sup>16,17</sup> – which only requires information about energies at the current time step. The other is a somewhat more involved formalism, denoted augmented fewest switches surface hopping (AFSSH) and introduced by Subotnik and co-workers.<sup>20,62</sup> The essence of the AFSSH method is that it explicitly propagates auxiliary trajectories on the potential surfaces that are not active in the dynamics.

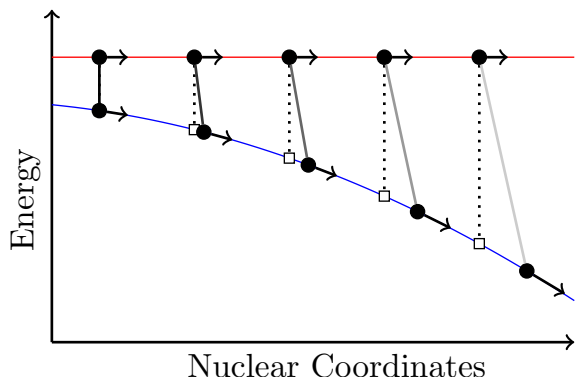


Figure 3: Depiction of an electronic wavepacket propagating on two coupled potential energy surfaces. The solid circles represent the true behaviour of the system: the part of the wavepacket on the lower surface moves faster than the part on the upper surface and therefore the two branches of the wavepacket lose coherence. The empty squares on  $S_1$  represent the artificially overcoherent state present in surface hopping dynamics and illustrate the need for applying a decoherence correction.

The EDC method<sup>18</sup> proceeds by defining a decoherence time

$$\tau_{\alpha\lambda} = \frac{\hbar}{|E_\alpha - E_\lambda|} \left( 1 + \frac{C}{E_{kin}} \right) \quad (6)$$

where  $E_\lambda$  and  $E_\alpha$  are the potential energies of the active surface  $\lambda$  and any other state  $\alpha$ ,  $E_{kin}$  is the kinetic energy, and  $C$  is an adjustable parameter usually set as  $C = 0.1$  H.**Sebastian: ?** The decoherence time  $\tau_{\alpha\lambda}$  is used to continu-

ously damp the coefficients of all non-active states in each time step. To this aim,  $c_\alpha$  is replaced by  $c_\alpha e^{-\frac{\Delta t}{\tau_{\alpha\lambda}}}$  and the coefficient of the active state is then rescaled such that its phase is kept and the total population of all states is 1.

In the simplified version<sup>20</sup> of the AFSSH formalism the decoherence rate is computed as

$$\frac{1}{\tau_{\alpha\lambda}} = \frac{(\mathbf{F}_{\alpha\alpha} - \mathbf{F}_{\lambda\lambda}) \cdot (\delta\mathbf{R}_\alpha - \delta\mathbf{R}_\lambda)}{2\hbar} \frac{2|\mathbf{F}_{\alpha\lambda} \cdot (\delta\mathbf{R}_\alpha - \delta\mathbf{R}_\lambda)|}{\hbar} \quad (7)$$

where  $\mathbf{F}_{\alpha\lambda}$  is defined as  $-\langle \Psi_\alpha | \nabla \hat{H} | \Psi_\lambda \rangle$  and  $\delta\mathbf{R}_\alpha$  is the position of the auxiliary trajectory belonging to state  $\alpha$ . These auxiliary trajectories are propagated in a diabatic picture using a force that is proportional to the state population  $|c_\alpha|^2$  as described in Ref. 20. The second term in Eq. (7) requires the evaluation of nonadiabatic coupling terms at every time step. In order to lift this requirement, we project the term onto the nuclear velocity  $\mathbf{v}$  and discretize the derivative to obtain

$$\frac{2|H_{\alpha\lambda} \times \mathbf{v} \cdot (\delta\mathbf{R}_\alpha - \delta\mathbf{R}_\lambda)|}{\Delta t \times \hbar |\mathbf{v}|^2} \quad (8)$$

Here,  $H_{\alpha\lambda}$  is an element of the locally diabatic Hamiltonian<sup>23</sup> that is already used for wavefunction propagation in SHARC.<sup>9</sup> Note that Eq. (8) is slightly modified with respect to Ref. 20.

AFSSH proceeds by computing the decoherence times for every inactive state and collapsing its amplitude to zero according to a stochastic algorithm.<sup>20</sup> In addition, two *ad hoc* criteria are introduced to cause a reset of the auxiliary trajectories without decoherence: (i) after every surface hop and (ii) according to a reset-time derived from the first term of Eq. (8).<sup>20</sup>

As final point, it is important to realise that these decoherence corrections only help to describe how the wavepacket divides into independent branches. Should these branches meet again later, there is no way to describe their interference correctly with independent trajectories.

## 2.4 Momentum rescaling and frustrated hops


A surface hopping algorithm ultimately has to describe the post Born-Oppenheimer exchange of energy between nuclear and electronic degrees of freedom. Practically, this occurs through the momentum rescaling process that is associated with surface hops. A number of different strategies have been devised  this purpose. Here, we will consider four of these possibilities, depending which quantity is conserved in the hop.<sup>33</sup> It is possible to impose conservation of the total energy  $E$ , the nuclear momentum  $\mathbf{p}$ , or both. Further, if both quantities are conserved, then one has to allow at least one degree of freedom where the momentum can change; this can be done along the nonadiabatic coupling (NAC) vector  $\mathbf{h}_{\alpha\lambda} = \mathbf{F}_{\alpha\lambda}/(E_\alpha - E_\lambda)$  or the gradient difference vector  $\mathbf{g}_{\alpha\lambda} = \mathbf{F}_{\alpha\alpha} - \mathbf{F}_{\lambda\lambda}$ . The four different momentum rescaling schemes are summarised in Table 1. In the  $E$  scheme the energy is conserved and the full momentum vector is rescaled along the momentum. In the  $\mathbf{p}$  scheme, the momentum is conserved, which means that no rescaling is performed at all. In the  $E\mathbf{p}_\mathbf{h}$  and  $E\mathbf{p}_\mathbf{g}$  schemes, the momentum is rescaled along the  $\mathbf{h}_{\alpha\lambda}$  and  $\mathbf{g}_{\alpha\lambda}$  directions, respectively.

Table 1: Methods for momentum rescaling investigated in this work.


	Conserved quantity	Rescaling along
$E$	Energy	Momentum
$\mathbf{p}$	Momentum	None
$E\mathbf{p}_\mathbf{h}$	Energy and momentum	NAC
$E\mathbf{p}_\mathbf{g}$	Energy and momentum	Grad. diff.

Based on formal arguments<sup>7,63,64</sup> and numerical results on model systems,<sup>29,65</sup> a number of authors have concluded that  $E\mathbf{p}_\mathbf{h}$  is the most rigorous option. Here We shall investigate whether this conclusion holds for a larger system containing many degrees of freedom, as  $[\text{Re}(\text{im})(\text{CO})_3(\text{phen})]^+$ , and how strong the effect is. From a practical viewpoint it is worth noting that  $E\mathbf{p}_\mathbf{h}$  is the only protocol that requires the availability of nonadiabatic coupling

vectors, which are not as readily available as energies and gradients do.

Whereas momentum conservation ( $\mathbf{p}$ ) during a hop is always possible and energy conservation ( $E$ ) is almost always possible for a large system as the one considered here, it is often not possible to conserve both at the same time fulfilling either the  $E\mathbf{p}_\mathbf{h}$  or  $E\mathbf{p}_\mathbf{g}$  conditions. Such cases, where a surface hop should occur according to the electronic Schrödinger equation but momentum rescaling is not possible, are termed frustrated hops. It has been argued that frustrated hops are required to maintain quantum detailed balance, i.e., the statistical ratio of up and down transitions between different energy surfaces.<sup>29,30,65</sup> Only by rejecting upward hops is it possible to assure that the lower energy state has increased population in agreement with the Boltzmann distribution.<sup>29,30</sup>

In the case of a frustrated hop the active state does not change. There are two options about what to do with the momentum and these options will be denoted  $+$  and  $-$ . In the  $+$  method the momentum is left unaltered, i.e. nothing at all happens after a frustrated hop. In the  $-$  method a portion of the momentum is reflected, which effectively means that the trajectory obtains a second chance to pass through the coupling region and perform a hop to the upper surface.

Specifically, we reflect the momentum parallel to the  $\mathbf{h}$  or  $\mathbf{g}$  vectors for the  $E\mathbf{p}_\mathbf{h}$  and  $E\mathbf{p}_\mathbf{g}$  methods, respectively. Following Refs 20,  this reversion is only done if the following two conditions are fulfilled:

$$(\mathbf{F}_\lambda \cdot \mathbf{f}_{\lambda\alpha})(\mathbf{F}_\alpha \cdot \mathbf{f}_{\lambda\alpha}) < 0 \quad (9)$$

$$(\mathbf{F}_\alpha \cdot \mathbf{f}_{\lambda\alpha})(\mathbf{p} \cdot \mathbf{f}_{\lambda\alpha}) < 0 \quad (10)$$

Here  $\lambda$  is the current state of the dynamics and  $\alpha$  is the state the trajectory would have reached through the frustrated hop;  $\mathbf{f}_{\lambda\alpha}$  refers to  $\mathbf{h}_{\lambda\alpha}$  or  $\mathbf{g}_{\lambda\alpha}$  for the  $E\mathbf{p}_\mathbf{h}$  and  $E\mathbf{p}_\mathbf{g}$  methods, respectively. The reversal proceeds by reversing the velocity for the atoms individually, thus conserving  $|\mathbf{p}|$  and  $E$  in the frustrated hop.

**new:** We denote the resulting protocols  $E\mathbf{p}_\mathbf{h}^+$ ,  $E\mathbf{p}_\mathbf{h}^-$ ,  $E\mathbf{p}_\mathbf{g}^+$ , and  $E\mathbf{p}_\mathbf{g}^-$ . In the case of  $E$ , it would in principle also be possible to apply the  $-$  pro-

TOCOL but we only evaluate + here (i.e.  $E$  implicitly means  $E^+$ ) for two reasons. First, the number of frustrated hops is small anyway. Second, an application of the  $E^-$  method would imply to revert the full momentum, which means that the whole trajectory simply proceeds in reverse after the frustrated hop.

## 2.5 Computational Details

Vibronic coupling parameters are obtained from electronic structure calculations performed using the B3LYP functional (as defined by Frisch and coworkers<sup>66</sup>) and all electron triple- $\zeta$  basis set.<sup>67</sup> The scalar relativistic effects were taken into account within the zeroth-order regular approximation (ZORA).<sup>68</sup> The vertical transition energies for 2 singlets and 4 triplet states were computed with TDDFT<sup>69,70</sup> at the same level described above under the Tamm-Damcoff approximation.<sup>71</sup> The non-equilibrium solvation within the linear-response TD-DFT with a high-frequency dielectric constant of 1.77 for water was used. The SOC effects were introduced according to a simplified relativistic perturbative TD-DFT formalism.<sup>72,73</sup> These electronic-structure calculations were done with the ADF2013 code.<sup>74</sup>

The model multi-dimensional PES are built from the vibrational normal modes of the singlet electronic ground state. From the 108 normal modes of  $[\text{Re}(\text{im})(\text{CO})_3(\text{phen})]^+$ , 15 were selected as the most important ones involved in the excited state decay starting at  $2^1\text{MLCT}$ , as described in Ref. 51. The resulting 15-mode model Hamiltonian accounts for 12 a' modes at 93, 235, 439, 498, 552, 637, 1174, 1336, 1444, 1554, 1623, 1660  $\text{cm}^{-1}$ , and for 3 a'' modes at 90, 475 and 626  $\text{cm}^{-1}$ , which correspond mainly to metal-carbonyl modes and vibrations localized on the phenanthroline ligand.<sup>51</sup> The model parameters corresponding to the excited state energies, SOC values, and intrastate and interstate coupling constants associated to those modes are reported in Ref. 52. All parameters used are supplied along with the output data via an external repository.<sup>75</sup>

The time-dependent Schrödinger equation for the nuclei was solved by employing the

MCTDH method.<sup>45-47</sup> The multiconfiguration nuclear wave-function is expressed as a linear combination of the Hartree products of the time-dependent basis functions, known as single-particle functions. The wavepacket ansatz adapted to the present non-adiabatic problem corresponds to the multiset formulation. The mode combination, number of primitive basis and single particle functions used in the simulations is the same as in Ref. 52. Harmonic-oscillator basis sets were employed. The initial wavepacket corresponds to the harmonic vibrational ground state of the electronic ground state, promoted at time zero to the  $2^1\text{MLCT}$  absorbing state. The calculations are done with the Heidelberg MCTDH Package (version 8.4.10).<sup>76</sup>

All surface hopping dynamics simulations were performed in the diagonal representation [Fig. 1 (c)] meaning that SOC is included in the PES. For the analysis, the results were transformed back into the diabatic representation as explained in Ref. 77, summing over the three triplet components. The initial conditions for the dynamics were created according to a Wigner distribution of the zero-point vibrational wavefunction within a harmonic approximation.<sup>78</sup> The electronic wavefunction was prepared in the diabatic  $2^1\text{MLCT}$  state and the initial active state of the trajectory was the diagonal surface most closely resembling this state. Note that this is a non-standard option within SHARC requiring manual adjustment of the initial wavefunction coefficients. A nuclear time step of 0.5 fs was chosen and the trajectories were propagated during 500 fs. A locally diabatic propagation for the wavefunctions was chosen<sup>23</sup> using 25 substeps per time step. For the decoherence correction we used the EDC method [Eq. (6),  $C=0.1$  H], the simplified AF-SSH method,<sup>20</sup> or no correction. Momentum rescaling was performed according to the four options presented in Tab. 1 and the + and - versions for treating frustrated hops as defined in Section 2.4 were used.

The quality of the dynamics was gauged by computing a time-averaged absolute error of the diabatic populations computed with surface hopping against the MCTDH reference, defined



as

$$\epsilon_{t_{max}} = \frac{\Delta t}{t_{max}} \sum_{t=\Delta t}^{t_{max}} \sum_{\alpha=1}^{N_{st}} |p_{\alpha}(t) - p_{\alpha}^{ref}(t)|. \quad (11)$$

Here,  $p_{\alpha}(t)$  is the population of state  $\alpha$  at time  $t$  and  $p_{\alpha}^{ref}(t)$  corresponds to the reference value computed with MCTDH. In the case of triplet states, the  $p_{\alpha}(t)$  value corresponds to the sum over all three components of the state. Two values of  $t_{max}$  are considered: 5 fs to evaluate the accuracy during the very early dynamics, and 500 fs. Accordingly, the maximum possible value for the error is 2, which would be obtained if there is no coincidence at all between the states populated in the two runs.

As an alternative error measure, time constants were obtained by fitting first-order kinetics models to the population data. Errors of the time constants were obtained with the bootstrapping method,<sup>79</sup> using 1000 bootstrapping samples for each ensemble.

### 3 Results

We start by discussing the states involved in the dynamics and their main dynamical features, as determined by the MCTDH method. Subsequently, we shall evaluate the performance of different surface hopping methods on the full model describing  $[\text{Re}(\text{im})(\text{CO})_3(\text{phen})]^+$  and various simplified models.

In line with previous work on this complex,<sup>51,52</sup> we will consider two singlet states and four triplet states (i.e. a total of 14 individual spin-orbit coupled states). All but one are of predominant MLCT character with the remaining one of IL character. In Table 2, the vertical excitation energies of these states are presented. Two types of labels are given to account for the MCH (labelled by energy, i.e.  $S_1, S_2, T_1 - T_4$ ) and diabatic (labelled by character, e.g.  $2^1\text{MLCT}$  for the second singlet MLCT state) representations (cf. Fig. 2). Table 2 shows that the six states occupy a narrow energy range of only 0.5 eV, suggesting rapid nonadiabatic transitions.

To simulate the dynamics of the complex after

Table 2: Singlet and triplet vertical excitations of the  $[\text{Re}(\text{im})(\text{CO})_3(\text{phen})]^+$  complex: energies and state labels in the MCH and diabatic representations.

MCH	Diabatic	$\Delta E$ (eV)
$S_1$	$1^1\text{MLCT}$	3.12
$S_2$	$2^1\text{MLCT}$	3.40
$T_1$	$1^3\text{MLCT}$	2.98
$T_2$	$2^3\text{MLCT}$	3.07
$T_3$	$1^3\text{IL}$	3.24
$T_4$	$3^3\text{MLCT}$	3.42

vertical excitation, the system was prepared in the diabatic  $2^1\text{MLCT}$  state and propagated for 500 fs. In Fig. 4 (a) dynamics computed at the MCTDH level of theory is presented. The first process observed is an ultrafast transfer of population from  $2^1\text{MLCT}$  to the almost quasidegenerate  $3^3\text{MLCT}$  state mediated via SOC and after only 12 fs the population of  $2^1\text{MLCT}$  has already decayed to 0.5. The  $3^3\text{MLCT}$  state reaches a maximum at only 24 fs and subsequently decays while populating the other triplet states and also transferring back some of the population to  $2^1\text{MLCT}$ . After 500 fs about 60% of the population is in  $1^3\text{MLCT}$  while the remaining part is about evenly split between  $2^3\text{MLCT}$  and  $1^3\text{IL}$ .

Figure 4 (b) shows the evolution of the same dynamics obtained with surface hopping and selecting the EDC/ $E\mathbf{p}_h^-$  option. At this level the agreement between surface hopping and MCTDH is very good and all the features mentioned above are well reproduced. The use of SHARC allows us to easily convert these results into the MCH representation, which is shown in Fig. 4 (c). The MCH populations closely resemble the diabatic ones with the exception that the lower energy states have larger populations than their corresponding diabatic states; for example, the rise of  $T_4$  in the early dynamics is somewhat lower than the rise of  $3^3\text{MLCT}$  and the population of  $T_1$  at the end of the simulated period is somewhat larger than the population of  $1^3\text{MLCT}$ . This is nevertheless expected as high-energy diabatic states mix with lower-lying energy states. **moved up:** We also want to briefly address the question of how

much the truncation of the model to 15 modes affects the overall dynamics within the LVC approximation. For this purpose, we recomputed the surface hopping dynamics including all 108 normal modes of  $[\text{Re}(\text{im})(\text{CO})_3(\text{phen})]^+$  and the corresponding linear vibronic coupling constants. The results, determined at the  $\text{EDC}/E\mathbf{p}_h^-$  level, are presented in Fig. 4 (d). This figure closely represents the corresponding results for the 15-mode model (Fig. 5 (b)) with only a few exceptions, e.g. the rise of  $3^3\text{MLCT}$  in the early dynamics is somewhat less pronounced and there is no second rise of  $2^1\text{MLCT}$ . We therefore conclude that the 15-mode model is a reasonable approximation of the overall complex, at least within a harmonic approximation.

We are now in the position to address the main concern of this work: How well are these processes reproduced by using different approximations within the surface hopping method? For this purpose, we have evaluated the surface hopping dynamics using 13 different levels of theory, where the decoherence correction, the mode of momentum rescaling and the treatment of frustrated hops are varied. The results are summarised in Fig. 5, see also the individual results in Figures S1-S13 of the supporting information. The bars of Fig. 5 are computed as floating averages on a logarithmic time scale considering the following intervals 0-1 fs, 1-2 fs, 2-4 fs, 4-8 fs until 256-500 fs, and coloured according to their electronic and spin character. The upper left panel displays compactly the MCTDH results from Fig. 4 (a). Here, one can see the initial population of  $2^1\text{MLCT}$ , which is the dominant state until the fifth bar (the interval 8-16 fs). Then, the  $3^3\text{MLCT}$  state dominates (16-32 fs) while in the final interval more than 50% of the population is in the  $1^3\text{MLCT}$  state.

Gratefully, all the methods considered show an appropriate time scale for the  $2^1\text{MLCT}$  decay and correctly predict the intermediate rise of  $3^3\text{MLCT}$ . However, most of them fall short when describing the outcome at the end of the dynamics and only the  $\text{EDC}/E\mathbf{p}_h^-$  correctly places more than 50% of the population in the  $1^3\text{MLCT}$  state, closely followed by

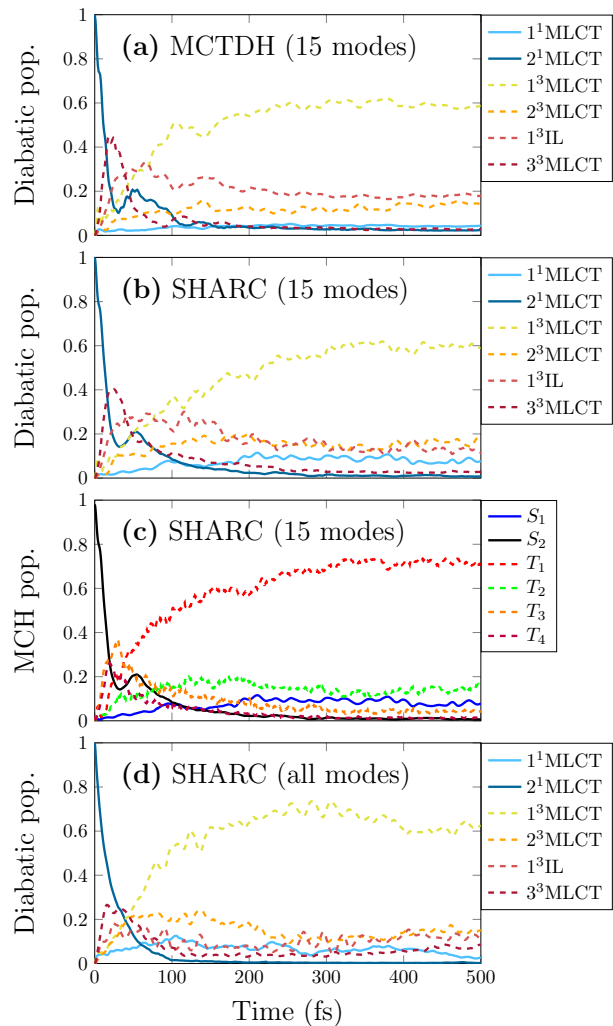


Figure 4: Time-evolution of the state populations of the full model considering (a) diabatic populations at the MCTDH level (15 modes), (b) diabatic populations (15 modes), (c) MCH populations (15 modes), (d) diabatic populations (all modes) at the surface hopping ( $\text{EDC}/E\mathbf{p}_h^-$ ) level.

the  $\text{EDC}/E\mathbf{p}_h^+$  and  $\text{EDC}/E\mathbf{p}_g^-$  methods (49% each).

To provide a more quantitative discussion of the deviations we compute the mean-absolute error  $\epsilon_{t_{max}}$  [Eq. (11)] for the times  $t_{max}=5$  and 500 fs. When considering the whole time span of 500 fs, the lowest error (marked by \* in Fig. 5) is obtained for  $\text{EDC}/E\mathbf{p}_h^-$  with  $\epsilon_{500} = 0.178$  followed, again, by  $\text{EDC}/E\mathbf{p}_h^+$  and  $\text{EDC}/E\mathbf{p}_g^-$ . Our implementation of the AF-SSH method performs surprisingly bad for this system and none of the  $\epsilon_{500}$  values are below 0.500. Not applying any decoherence correc-

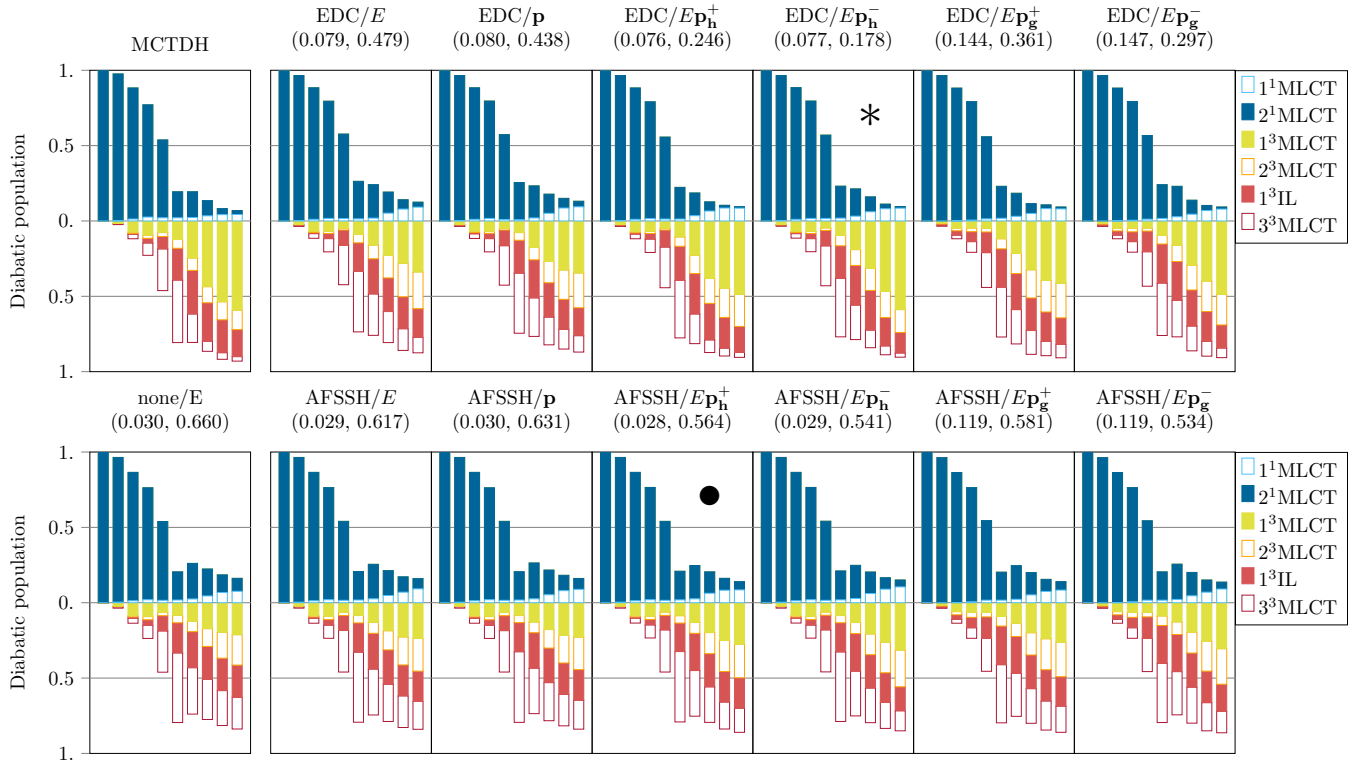


Figure 5: Diabatic electronic populations for the full model as a function of time considering different surface hopping algorithms plotted on a logarithmic time scale for 0-500 fs after photoexcitation. Mean-absolute errors computed for the first 5 fs and for the whole dynamics are given in parentheses ( $\epsilon_5, \epsilon_{500}$ ) and the best performers over these two timescales are marked by  $\bullet$  and  $*$ , respectively.

tion “none/E” performs worst over the full time scale with an error of 0.660. The picture is reversed when just the first 5 fs are considered. In this case all the EDC methods have errors over 0.075 while the AFSSH methods, with the exception of  $E\mathbf{p}_g$ , have errors below 0.030 and the best result ( $\bullet$ ) is obtained for  $E\mathbf{p}_h^+$ . Interestingly, not applying any decoherence correction performs well for the first 5 fs indicating that at this short time scale a coherent propagation of the electron wavefunction is adequate. Although a detailed discussion will be done in the next section, we emphasise now that the errors introduced by the different surface hopping algorithms are non-negligible and that apparent unimportant algorithmic details do affect the results strongly.

Noting the challenges involved in the full model of  $[\text{Re}(\text{im})(\text{CO})_3(\text{phen})]^+$ , where the interactions of 14 spin-orbit coupled states have to be modelled correctly, we want now to get a deeper insight into the effect of the different implementations by studying simpler models. For

this purpose, we use the same set of parameterized 15 normal modes but a smaller number of states. First, we consider only the two singlet states  $1^1\text{MCLT}$  and  $2^1\text{MCLT}$ . As seen in the upper left panel of Fig. 6, the interconversion between these two states happens on the time scale of a few hundred femtoseconds and for the last two bars, i.e. the time after 128 fs, more than 50% of the population is in  $1^1\text{MCLT}$ . It can be readily seen that the interconversion is too slow with all surface hopping protocols as none of them has two bars below the line indicating a population of 0.5. Interestingly, the EDC protocols have significantly enhanced error bars when compared to their AFSSH counterparts. For this model, the AFSSH/ $E\mathbf{p}_h^-$  method gives the best performance considering both  $\epsilon_5$  and  $\epsilon_{500}$ .

We systematically increase the complexity of the model, considering the interaction between the  $2^1\text{MCLT}$  and  $1^3\text{IL}$  states that gives rise to four spin-orbit coupled states. The upper left panel of Fig. 7 shows that intersystem crossing

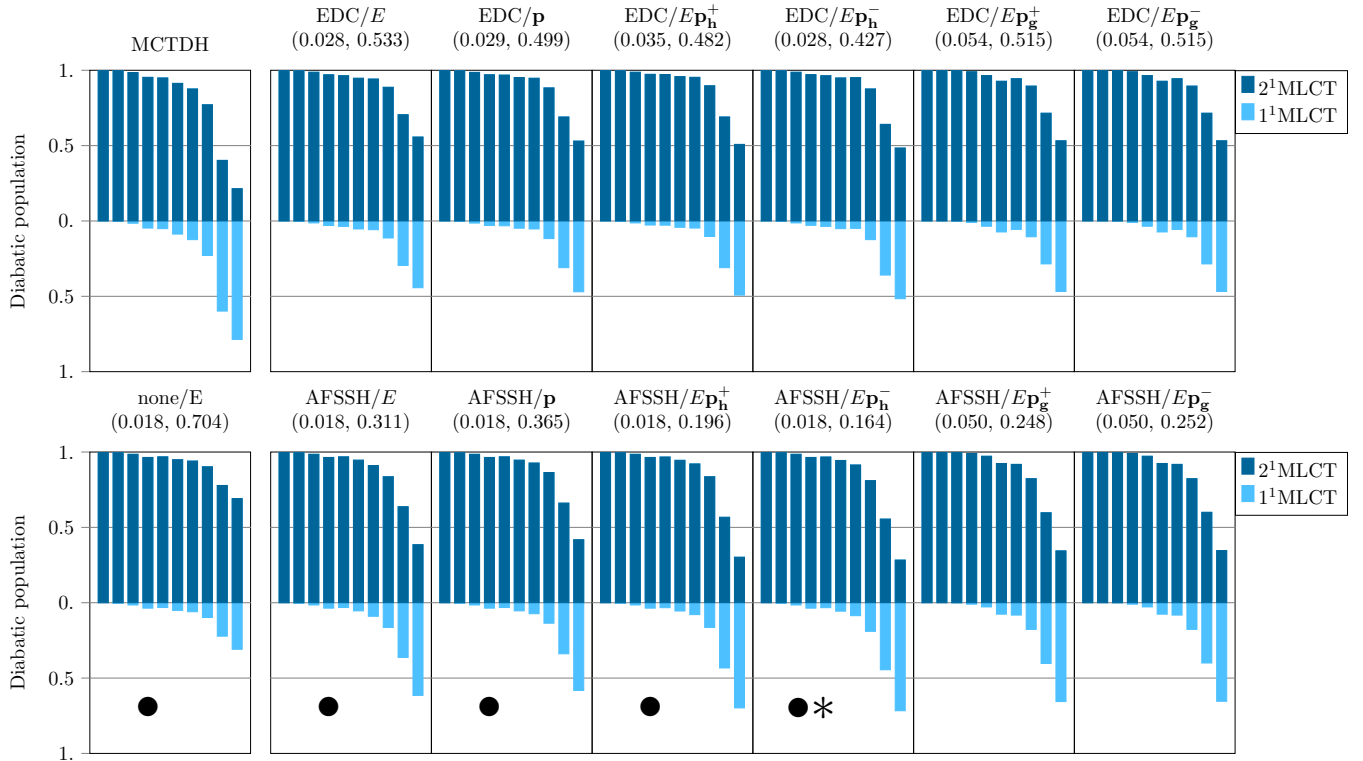


Figure 6: Diabatic electronic populations considering the singlet MCLT states as a function of time considering different surface hopping algorithms plotted on a logarithmic time scale for 0-500 fs after photoexcitation. Mean-absolute errors computed for the first 5 fs and for the whole dynamics are given in parentheses ( $\epsilon_5, \epsilon_{500}$ ) and the best performers over these two timescales are marked by • and \*, respectively.

should occur on a similar time scale to the internal conversion of the previous case. However, the underlying physics is clearly different as  $2^1\text{MCLT}$  and  $1^3\text{IL}$  are coupled via SOC whereas the singlet states in Fig. 6 are connected by non-relativistic vibronic coupling. In addition, the position of the minimum of the  $1^3\text{IL}$  potential surface is significantly altered when compared to the MLCT states.<sup>51</sup> As a consequence of these changes in parameters, strongly varying outcomes are observed for the different surface hopping methods. In general, improved results are obtained with respect to the previous case and most methods show acceptable error bars. Surprisingly, the only severe outliers are the  $E\mathbf{p}_h^+$  and  $E\mathbf{p}_g^+$  protocols, which exhibit strongly enhanced errors through overestimating the intersystem crossing rate when compared to all other methods. Again, this underlines how a seemingly innocuous methodological detail, such as the  $+/-$  treatment of frustrated hops can have severe consequences. The best re-

sult over the full time scale (\*) is obtained for EDC/ $\mathbf{p}$ , closely followed by EDC/ $E\mathbf{p}_h^-$  while for the first 5 fs, AFSSH/ $\mathbf{p}$  and AFSSH/ $E\mathbf{p}_h^-$  are in the lead. Interestingly, the  $\mathbf{p}$  method, meaning that no momentum rescaling is performed at all after a hop, performs very well here.

Finally, we consider the  $3^3\text{MLCT}$  and  $1^3\text{IL}$  states, which gives rise to 9 states interacting via SOC and vibronic coupling, see Fig. 8. In this case the interconversion occurs somewhat faster than in the previous cases and after 42 fs half the population is already in the  $1^3\text{IL}$  state according to the MCTDH reference. Most of the surface hopping protocols perform reasonable well in this case with  $\epsilon_5$  values below 0.01 and  $\epsilon_{500}$  below 0.20. However, in this case the  $E\mathbf{p}_g$  methods are significantly away from the others with long-time errors above 0.40. The best performing methods over 5 fs (•) and 500 fs (\*) are AFSSH/ $E\mathbf{p}_h^+$  and EDC/ $E\mathbf{p}_h^+$ , respectively.

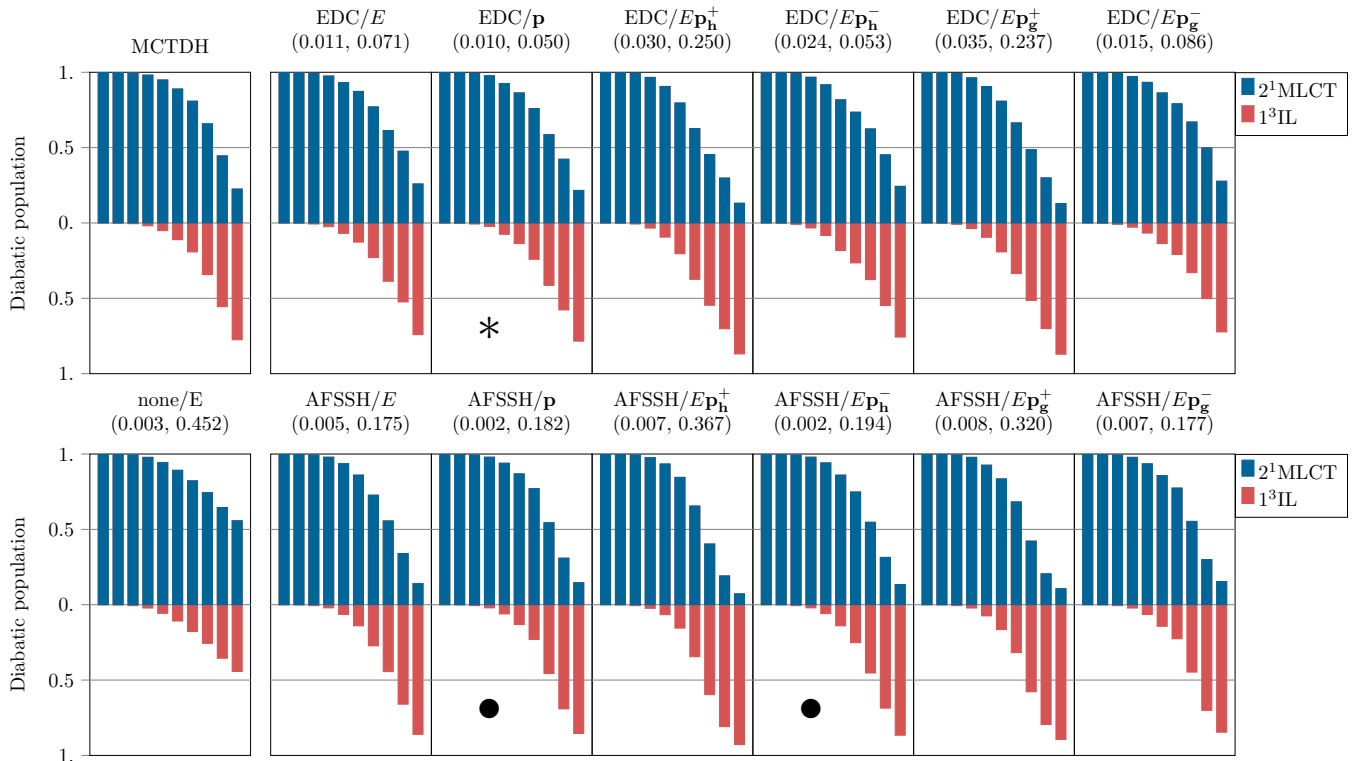


Figure 7: Diabatic electronic populations considering the  $2^1\text{MLCT}$  and  $1^3\text{IL}$  states as a function of time considering different surface hopping algorithms plotted on a logarithmic time scale for 0-500 fs after photoexcitation. Mean-absolute errors computed for the first 5 fs and for the whole dynamics are given in parentheses  $(\epsilon_5, \epsilon_{500})$  and the best performers over these two timescales are marked by  $\bullet$  and  $*$ , respectively.

A more compact form of the results is presented in Table 3, where the  $\epsilon_5$  and  $\epsilon_{500}$  values of the four types of dynamics are averaged. Accordingly, one finds that the  $\text{EDC}/E\mathbf{p}_h^-$  method clearly outperforms all other protocols, closely followed by  $\text{AFSSH}/E\mathbf{p}_h^-$  and  $\text{EDC}/E\mathbf{p}_h^+$ . If high precision is required in the early part of the dynamics, then EDC somewhat overcorrects and one of the AFSSH protocols is preferable where the lowest errors are obtained for  $\text{AFSSH}/E\mathbf{p}_h$  in its + and - versions. In general, we observe that the most rigorous, yet the computationally most involved,  $E\mathbf{p}_h$  method clearly outperforms the others. We also observe a clear trend in the way that frustrated hops are treated where - outperforms +. The comparison between EDC and AFSSH is not so clear but there is a slight preference for EDC.

A complementary perspective of the dynamics can be achieved by fitting time constants. For this purpose, the following kinetic models

were considered

$$S_2 + S_1 \rightleftharpoons T_4 + T_3 + T_2 + T_1 \quad (12)$$

$$S_2 \rightarrow S_1 \quad (13)$$

$$S_2 \rightarrow T_3 \quad (14)$$

$$T_4 \rightleftharpoons T_3 \quad (15)$$

and the data fitted appropriately. In all these cases, the decay times for the forward reaction were compared although for Eq. (12) and Eq. (15) we also fitted the backwards reaction rate. The obtained times are plotted in Fig. 9 on a logarithmic scale. The dotted lines indicate the reference values computed at the MCTDH level and the shaded areas indicate  $\pm 25\%$  error windows. **corresponding to values between 3/4 and 4/3 times the reference time.** In the case of the full model, we fitted the overall intersystem crossing as a reversible interconversion between singlets and triplets [cf. Eq. (12)]. The reference time

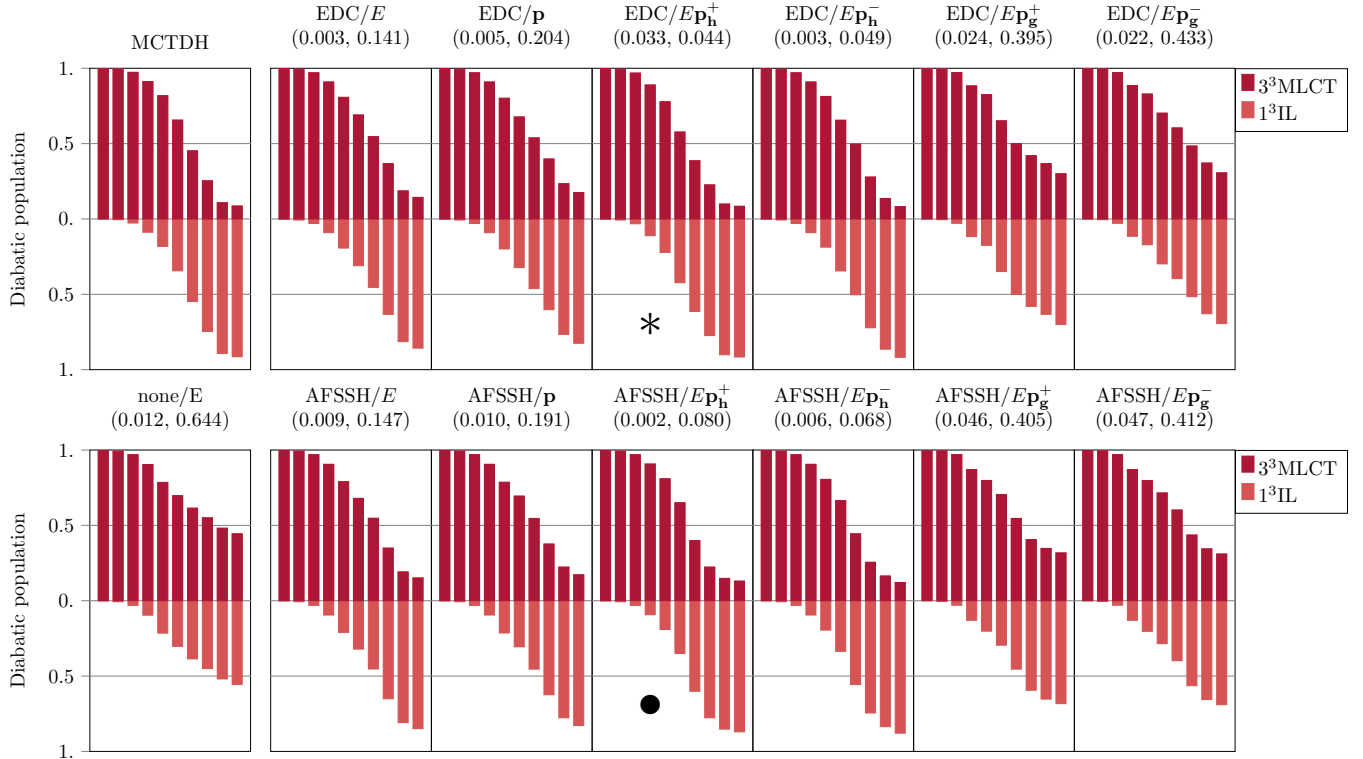


Figure 8: Diabatic electronic populations considering the  $3^3\text{MLCT}$  and  $1^3\text{IL}$  states as a function of time considering different surface hopping algorithms plotted on a logarithmic time scale for 0-500 fs after photoexcitation. Mean-absolute errors computed for the first 5 fs and for the whole dynamics are given in parentheses  $(\epsilon_5, \epsilon_{500})$  and the best performers over these two timescales are marked by  $\bullet$  and  $*$ , respectively.

for the forward intersystem crossing was determined as 16.0 fs. All the surface hopping simulations stay well within the indicated error window and deviate less than 2 fs from this result. The  $2^1\text{MLCT}/1^1\text{MLCT}$  system decays with a time constant of 235 fs for MCTDH. Interestingly, all the surface hopping protocols overshoot this value and  $\text{AFSSH}/E\mathbf{p}_h^-$  is the only method within the specified error window. The  $2^1\text{MLCT}/1^3\text{IL}$  interconversion occurs on a very similar time scale to the previous case at the MCTDH level (239 fs). As opposed to the previous case, most of the employed surface hopping methods underestimate this time and four methods are within the error window:  $\text{EDC}/E$ ,  $\text{EDC}/\mathbf{p}$ ,  $\text{EDC}/E\mathbf{p}_h^-$ , and  $E\mathbf{p}_g^-$ . The interconversion between  $3^3\text{MLCT}$  and  $1^3\text{IL}$  occurs with a time constant of 57 fs at the MCTDH level. This time constant is generally overestimated by surface hopping, with the best time constants provided by the  $E\mathbf{p}_h^+$  protocol using either the EDC or AFSSH decoherence correc-

tion.

Figure 9 evidences that none of the surface hopping protocols places all four time constants within the given error window; the only protocol that keeps at least three out of the four time constants within the specified error window is  $\text{AFSSH}/E\mathbf{p}_h^-$ . Moreover, one sees that the errors are generally not uniform as the time scales are sometimes overestimated and sometimes underestimated, showing that there is probably no simple solution. An interesting trend is the fact that all the  $+$  methods decay on shorter time scales than the  $-$  methods. This may be understood in the following simple picture: The  $-$  protocol redirects the trajectory into the crossing region after a frustrated hop. Thus, the trajectory obtains a second chance to hop up into the higher state, which leads to the fact that the overall decay to the lower state is slowed down.

Finally, it is of interest to discuss whether the results are statistically significant, i.e. whether

Table 3: Time-weighted mean absolute errors averaged over the four types of trajectories computed for the initial 5 fs and the full 500 fs of the dynamics.

$t_{max}$		$E$	$\mathbf{p}$	$E\mathbf{p}_h^+$	$E\mathbf{p}_h^-$	$E\mathbf{p}_g^+$	$E\mathbf{p}_g^-$
5 fs	EDC	0.030	0.031	0.043	0.033	0.064	0.059
	AFSSH	0.016	0.016	<b>0.015</b>	<b>0.015</b>	0.057	0.057
	none	0.017					
500 fs	EDC	0.306	0.298	0.255	<b>0.177</b>	0.377	0.333
	AFSSH	0.313	0.343	0.302	0.242	0.389	0.344
	none	0.616					

200 trajectories are enough to provide almost converged decay times. This is assessed using a **bootstrap algorithm**<sup>?</sup> that estimates the error related to the finite number of trajectories. The results are presented as error bars in the EDC/ $E$  panel shown on the left of Fig. 9. As these errors are significantly smaller than the fluctuations between the different methods, it is fair to assume that none of the conclusions would change if a significantly larger number of trajectories were run.

## 4 Discussion

The disparity of the data presented above illustrates the importance of the algorithmic details, and while it makes it difficult to draw a final conclusion, a number of clear trends emerge. For all the models considered and ways to evaluate the results, it is found that momentum rescaling along the nonadiabatic coupling vector ( $E\mathbf{p}_h$ ) is superior to the three other evaluated methods. It has been argued previously that this is the most rigorous way of momentum rescaling.<sup>7,63,64</sup> The main effect seen by the application of  $E\mathbf{p}_h$  is an enhanced number of frustrated hops, which lead to the fact that the trajectory correctly remains trapped in the lower state. This is similar to the results of Refs 29,30,65 which discuss this effect in terms of detailed balance. This effect is particularly drastic whenever a large number of states are present in a narrow energy window as is the case for transition metal complexes but will probably play a smaller role in the case

of a smaller number of well-separated states as usually found in small organic molecules. The challenge of applying the  $E\mathbf{p}_h$  protocol is that it requires the availability of nonadiabatic couplings, which are not straightforward to calculate with most of the electronic structure codes available. With this hurdle in mind, we have attempted the same protocol only replacing the nonadiabatic coupling with the gradient difference ( $E\mathbf{p}_g$ ). However, we found that this introduces significant errors and in many respects even performs worse than a simple rescaling along the momentum. A more pragmatic approach to solve the problem may be to introduce a new *ad hoc* criterion to reduce the number of upward hops, e.g. limiting the maximal hopping energy. But this option is out of the scope of this paper.

Considering that the number of frustrated hops is the main feature that sets the  $E\mathbf{p}_h$  and  $E\mathbf{p}_g$  methods apart from the others, we have evaluated different options of what to do after a frustrated hop in these two cases and found that reflection (-) generally outperforms completely ignoring the hops (+). The - protocol reflects the trajectory back into the crossing region and provides a second chance of hopping into the higher state. As a consequence, we find that the net transfer to the lower state is slowed down whenever the - protocol is used. As discussed above, the - protocol does not make much sense for simple rescaling along the momentum ( $E^-$ ) and was not investigated here.

Unfortunately, the question of decoherence correction does not have a straightforward answer. While we generally find that not applying

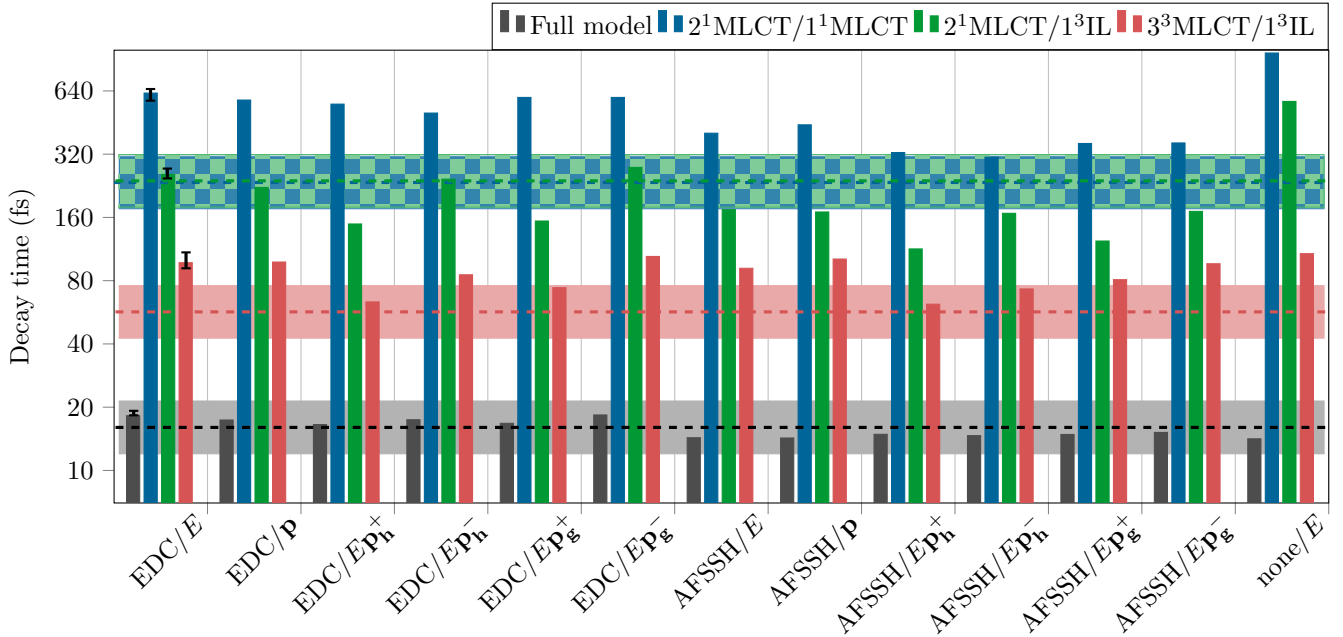


Figure 9: Fitted decay times for the different models and computational methods plotted on a logarithmic scale. The dashed lines and highlighted areas indicate MCTDH reference values (note that the reference values for  $2^1\text{MLCT}/1^1\text{MLCT}$  and  $2^1\text{MLCT}/1^3\text{IL}$  almost coincide and are, therefore, not distinguishable in this plot).

a decoherence correction leads to incorrect results, none of the EDC and AFSSH protocols provided satisfactory solutions. EDC overcorrected in the short time scale while the AFSSH method generally underestimated decoherence. The problem of these methods may be understood in the sense that neither of them is size-consistent in the present implementation. The EDC method [Eq. (6)] depends on the overall kinetic energy  $E_{kin}$  of the system. Adding non-interacting atoms to the system will increase the overall kinetic energy and thus reduce the decoherence time. In the case of AFSSH the argument is more subtle. Following Ref. 20, the positions and momenta of the auxiliary trajectories are reset after every surface hop. In the full model of the complex considered there are 14 states present within as little as 0.5 eV. As a consequence, an exorbitant number of hops occur, mostly related to trivial crossings, meaning that the auxiliary trajectories never have the time to properly build up to induce decoherence and as a consequence the decoherence rate is strongly underestimated. More generally, we can say that the AFSSH algorithm is not size-

consistent with respect to the density of states in the system as the addition of non-interacting electronic states to any model system will lower the decoherence rate through an enhanced number of surface hops. This problem might be solved by using a more sophisticated implementation of the AFSSH algorithm that treats trivial crossings differently from true surface hops. **[Sebastian: One could suggest that 1 minus the hop-inducing probability could be used as a reset probability, but if you do not want to add such speculations, it's also fine to me.]** However, for the present study we are left to conclude that AFSSH does not produce enhanced results compared to EDC despite its more involved formalism.

On the optimistic side, we find that for any of the models considered, there is at least one surface hopping protocol that produces satisfactory results, revealing that errors are not due to non-local quantum effects –which would invalidate the trajectory approximation as such– but rather to small methodological implementations of the surface hopping method. This work then illustrates that it is important to obtain



a deeper understanding of the effect of these methodological details. ~~Conversely, it would be interesting to see if improved results could be obtained by other on the fly dynamics approaches such as ab initio multiple spawning,<sup>4</sup> the coupled trajectory mixed quantum-classical scheme,<sup>37</sup> and variational multiconfigurational Gaussians.<sup>80</sup>~~

## 5 Conclusion

The purpose of this study was to evaluate the reliability of surface hopping dynamics in the challenging case of transition metal complexes, which are typically characterised by the presence of a high density of electronic states and a large number of crossings among them. For this purpose, we ~~constructed~~ a LVC model of the  $[\text{Re}(\text{im})(\text{CO})_3(\text{phen})]^+$  complex including 15 vibrational normal modes. Simulations were run on the full set of relevant states (2 singlets and 4 triplets) as well as on smaller subsets. Surface hopping simulations were run by varying three parameters in the algorithm –the mode of momentum rescaling, the treatment of frustrated hops, and the decoherence correction– and then compared against an MCTDH reference. It was clearly found that momentum rescaling along the coupling vector outperforms all other methods. Also a preference for reflecting the momentum after a frustrated hop was found. Neither of the two decoherence corrections applied were completely satisfactory but we found better results for the simple and robust EDC method.

**Acknowledgement** FP, SM and LG gratefully acknowledge funding from the Austrian Science Fund – Austria (FWF) within project I2883. MF, EG and CD thank the Labex CSC (ANR-10-LABX- 0026\_CSC) and the French/Austrian ANR-15-CE29-0027-01 DeNeTheor. The electronic structure calculations were performed at the Vienna Scientific Cluster, the High Performance Computer Centre (HPC) of the University of Strasbourg and nodes cluster of the Laboratoire de Chimie Quantique (CNRS/University of Strasbourg).

**Supporting Information Available:**

Time-dependent populations of the dynamics simulations for all methods and models (Figure S1-S52). The research data supporting this publication can be accessed via DOI: 10.17028/rd.lboro.c.4493135.v1.<sup>75</sup> This material is available free of charge via the Internet at <http://pubs.acs.org/>.

## References

- (1) Martínez, T. J. *Acc. Chem. Res.* **2006**, *39*, 119–126.
- (2) Plasser, F.; Barbatti, M.; Aquino, A. J. A.; Lischka, H. *Theor. Chem. Acc.* **2012**, *131*, 1073.
- (3) Nelson, T.; Fernandez-Alberti, S.; Roitberg, A. E.; Tretiak, S. *Acc. Chem. Res.* **2014**, *47*, 1155–1164.
- (4) Long, R.; Prezhdo, O. V.; Fang, W. *Wiley Interdiscip. Rev. Comput. Mol. Sci.* **2017**, *7*, e1305.
- (5) Oberhofer, H.; Reuter, K.; Blumberger, J. *Chem. Rev.* **2017**, *117*, 10319–10357.
- (6) Curchod, B. F. E.; Martínez, T. J. *Chem. Rev.* **2018**, *118*, 3305–3336.
- (7) Tully, J. C. *J. Chem. Phys.* **1990**, *93*, 1061–1071.
- (8) Kubar, T.; Elstner, M. *Phys. Chem. Chem. Phys.* **2013**, *15*, 5794.
- (9) Mai, S.; Marquetand, P.; González, L. *Int. J. Quantum Chem.* **2015**, *115*, 1215–1231.
- (10) Tavernelli, I. *Acc. Chem. Res.* **2015**, *48*, 792–800.
- (11) Subotnik, J. E.; Jain, A.; Landry, B.; Petit, A.; Ouyang, W.; Bellonzi, N. *Annu. Rev. Phys. Chem.* **2016**, *67*, 387–417.
- (12) Wang, L.; Akimov, A.; Prezhdo, O. V. *J. Phys. Chem. Lett.* **2016**, *7*, 2100–2112.
- (13) Spencer, J.; Scalfi, L.; Carof, A.; Blumberger, J. *Faraday Discuss.* **2016**, *195*, 215–236.

- (14) Crespo-Otero, R.; Barbatti, M. *Chem. Rev.* **2018**, *118*, 7026–7068.
- (15) Filatov, M.; Min, S. K.; Kim, K. S. *J. Chem. Theory Comput.* **2018**, *14*, 4499–4512.
- (16) Zhu, C.; Nangia, S.; Jasper, A. W.; Truhlar, D. G. *J. Chem. Phys.* **2004**, *121*, 7658–7670.
- (17) Zhu, C.; Jasper, A. W.; Truhlar, D. G. *J. Chem. Theory Comput.* **2005**, *1*, 527–540.
- (18) Granucci, G.; Persico, M. *J. Chem. Phys.* **2007**, *126*, 1–11.
- (19) Jaeger, H. M.; Fischer, S.; Prezhdo, O. V. *J. Chem. Phys.* **2012**, *137*, 22A545.
- (20) Jain, A.; Alguire, E.; Subotnik, J. E. *J. Chem. Theory Comput.* **2016**, *12*, 5256–5268.
- (21) Jasper, A. W.; Truhlar, D. G. *Chem. Phys. Lett.* **2003**, *369*, 60–67.
- (22) Plasser, F.; Granucci, G.; Pittner, J.; Barbatti, M.; Persico, M.; Lischka, H. *J. Chem. Phys.* **2012**, *137*, 22A514.
- (23) Granucci, G.; Persico, M.; Toniolo, A. *J. Chem. Phys.* **2001**, *114*, 10608–10615.
- (24) Plasser, F.; Crespo-Otero, R.; Pedrozoli, M.; Pittner, J.; Lischka, H.; Barbatti, M. *J. Chem. Theory Comput.* **2014**, *10*, 1395–1405.
- (25) Mai, S.; Atkins, A. J.; Plasser, F.; González, L. *submitted for publication* **2019**,
- (26) Müller, U.; Stock, G. *J. Chem. Phys.* **1997**, *107*, 6230–6245.
- (27) Landry, B. R.; Subotnik, J. E. *J. Chem. Phys.* **2012**, *137*, 22A513.
- (28) Chen, H. T.; Reichman, D. R. *J. Chem. Phys.* **2016**, *144*, 094104.
- (29) Käb, G. *J. Phys. Chem. A* **2006**, *110*, 3197–3215.
- (30) Parandekar, P. V.; Tully, J. C. *J. Chem. Phys.* **2005**, *122*.
- (31) Topaler, M. S.; Hack, M. D.; Allison, T. C.; Liu, Y.-P.; Mielke, S. L.; Schwenke, D. W.; Truhlar, D. G. *J. Chem. Phys.* **1997**, *106*, 8699–8709.
- (32) Topaler, M. S.; Allison, T. C.; Schwenke, D. W.; Truhlar, D. G. *J. Chem. Phys.* **1998**, *109*, 3321–3345.
- (33) Jasper, A. W.; Hack, M. D.; Truhlar, D. G. *J. Chem. Phys.* **2001**, *115*, 1804–1816.
- (34) Mignolet, B.; Curchod, B. F. E. *J. Phys. Chem. A* **2019**, *123*, acs.jpca.9b00940.
- (35) Plasser, F.; Lischka, H. *J. Chem. Phys.* **2011**, *134*, 34309.
- (36) Worth, G. A.; Hunt, P.; Robb, M. A. *J. Phys. Chem. A* **2003**, *107*, 621–631.
- (37) Min, S. K.; Agostini, F.; Tavernelli, I.; Gross, E. K. U. *The J. Phys. Chem. Letters* **2017**, *8*, 3048–3055.
- (38) Koppel, H.; Domcke, W.; Cederbaum, L. S. *Adv. Chem. Phys.* **1984**, *57*, 59–246.
- (39) Raab, A.; Worth, G. A.; Meyer, H.-D.; Cederbaum, L. S. *J. Chem. Phys.* **1999**, *110*, 936–946.
- (40) Krawczyk, R. P.; Malsch, K.; Hohlneicher, G.; Gillen, R. C.; Domcke, W. *Chem. Phys. Lett.* **2000**, *320*, 535–541.
- (41) Faraji, S.; Meyer, H.-D.; Köppel, H. *J. Chem. Phys.* **2008**, *129*, 074311.
- (42) Tamura, H.; Burghardt, I. *J. Am. Chem. Soc.* **2013**, *135*, 16364–16367.
- (43) Eng, J.; Gourlaouen, C.; Gindensperger, E.; Daniel, C. *Acc. Chem. Res.* **2015**, *48*, 809–817.
- (44) Fumanal, M.; Daniel, C. *J. Comput. Chem.* **2016**, *3*, 2454–2466.

- (45) Meyer, H.-D.; Manthe, U.; Cederbaum, L. *Chem. Phys. Lett.* **1990**, *165*, 73–78.
- (46) Beck, M. H.; Jäckle, A.; Worth, G. A.; Meyer, H.-D. *Phys. Rep.* **2000**, *324*, 1–105.
- (47) Meyer, H.-D., Gatti, F., Worth, G. A., Eds. *Multidimensional Quantum Dynamics: MCTDH Theory and Applications*; Wiley-VCH, 2009.
- (48) Plasser, F.; Gómez, S.; Menger, M. F. S. J.; Mai, S.; González, L. *PCCP* **2019**, *21*, 57–59.
- (49) Penfold, T. J.; Gindensperger, E.; Daniel, C.; Marian, C. M. *Chem. Rev.* **2018**, *118*, 6975–7025.
- (50) Harabuchi, Y.; Eng, J.; Gindensperger, E.; Taketsugu, T.; Maeda, S.; Daniel, C. *J. Chem. Theory Comput.* **2016**, *12*, 2335–2345.
- (51) Fumanal, M.; Gindensperger, E.; Daniel, C. *J. Chem. Theory Comput.* **2017**, *13*, 1293–1306.
- (52) Fumanal, M.; Gindensperger, E.; Daniel, C. *Phys. Chem. Chem. Phys.* **2018**, *20*, 1134–1141.
- (53) Fumanal, M.; Plasser, F.; Mai, S.; Daniel, C.; Gindensperger, E. *J. Chem. Phys.* **2018**, 124119.
- (54) Fumanal, M.; Gindensperger, E.; Daniel, C. *The Journal of Physical Chemistry Letters* **2018**, *9*, [acs.jpclett.8b02319](https://doi.org/10.1021/acs.jpclett.8b02319).
- (55) Mai, S.; Marquetand, P.; González, L. *Wiley Interdiscip. Rev. Comput. Mol. Sci.* **2018**, *8*, e1370.
- (56) Mai, S.; Plasser, F.; Marquetand, P.; González, L. In *Attosecond Molecular Dynamics*; Vrakking, M. J. J., Lepine, F., Eds.; Theoretical and Computational Chemistry Series; The Royal Society of Chemistry, 2019.
- (57) Mai, S.; Richter, M.; Ruckebauer, M.; Plasser, F.; Oppel, M.; Marquetand, P.; González, L. SHARC: Surface Hopping Including Arbitrary Couplings – Program Package for Non-Adiabatic Dynamics; available from <http://sharc-md.org>. 2014.
- (58) Worth, G. A.; Cederbaum, L. S. *Annu. Rev. Phys. Chem.* **2004**, *55*, 127–158.
- (59) Schuurman, M. S.; Yarkony, D. R. *J. Chem. Phys.* **2007**, *127*, 094104.
- (60) Tegmark, M. *Phys. Rev. E - Stat. Physics, Plasmas, Fluids, Relat. Interdiscip. Top.* **2000**, *61*, 4194–4206.
- (61) Zurek, W. H. *Rev. Mod. Phys.* **2003**, *75*, 715–775.
- (62) Subotnik, J. E.; Shenvi, N. *J. Chem. Phys.* **2011**, *134*, 30–45.
- (63) Herman, M. F. *J. Chem. Phys.* **1984**, *81*, 754–763.
- (64) Coker, D. F.; Xiao, L. *J. Chem. Phys.* **1995**, *102*, 496–510.
- (65) Carof, A.; Giannini, S.; Blumberger, J. *J. Chem. Phys.* **2017**, *147*.
- (66) Stephens, P. J.; Devlin, F. J.; Chabalowski, C. F.; Frisch, M. J. *J. Phys. Chem.* **1994**, *98*, 11623–11627.
- (67) Van Lenthe, E.; Baerends, E. J. *Journal of Computational Chemistry* **2003**, *24*, 1142–1156.
- (68) van Lenthe, E.; van Leeuwen, R.; Baerends, E. J.; Snijders, J. G. *International Journal of Quantum Chemistry* **1996**, *57*, 281–293.
- (69) Runge, E.; Gross, E. K. *Physical Review Letters* **1984**, *52*, 997–1000.
- (70) Petersilka, M.; Gossmann, U. J.; Gross, E. K. U. *Physical Review Letters* **1996**, *76*, 1212–1215.

- (71) Peach, M. J.; Tozer, D. J. *Journal of Physical Chemistry A* **2012**, *116*, 9783–9789.
- (72) Wang, F.; Ziegler, T.; van Lenthe, E.; van Gisbergen, S.; Baerends, E. J. *The Journal of Chemical Physics* **2005**, *122*, 204103.
- (73) Wang, F.; Ziegler, T. *The Journal of Chemical Physics* **2005**, *123*, 154102.
- (74) ADF, SCM, Theoretical Chemistry, Vrije Universiteit, Amsterdam, The Netherlands, 2013, online at <https://www.scm.com/Downloads/>.
- (75) Supporting research data available: Parameters (SHARC input format) and time-dependent populations from the dynamics simulations for all the models evaluated. <https://doi.org/10.17028/rd.lboro.c.4493135.v1>.
- (76) Meyer, H.-D. The MCTDH Package, version 8.4, University of Heidelberg, Heidelberg, Germany, 2007.
- (77) Mai, S.; Marquetand, P.; González, L. *J. Chem. Phys.* **2014**, *140*, 204302.
- (78) Dahl, J. P.; Springborg, M. *J. Chem. Phys.* **1988**, *88*, 4535–4547.
- (79) Nangia, S.; Jasper, A. W.; Miller, T. F.; Truhlar, D. G. *J. Chem. Phys.* **2004**, *120*, 3586–3597.
- (80) Richings, G. W.; Polyak, I.; Spinlove, K. E.; Worth, G. A.; Burghardt, I.; Lasorne, B. *Int. Rev. Phys. Chem.* **2015**, *34*, 269–308.

# Graphical TOC Entry

